Available online at www.sciencedirect.com
SCIENCE DIRECT®
Journal of Solid State Chemistry 177 (2004) 3575–3580
JOURNAL OF SOLID STATE CHEMISTRY
http://elsevier.com/locate/jssc

Why does uranium oxide phosphate contract on heating?

Gilles Wallez,[a,*] Suzanne Launay,[a] Michel Quarton,[a] Nicolas Dacheux,[b] and Jean-Louis Soubeyroux[c]

[a] *Laboratoire de Cristallochimie du Solide (CNRS-URA 1388), Université Pierre et Marie Curie-Paris VI, 4, place Jussieu, 75252, Paris Cedex 05, France*
[b] *Groupe de Radiochimie, IPN, Université Paris Sud, B. P. N° 1, 91406 Orsay, France*
[c] *Institut Laue-Langevin, 6 rue Jules Horowitz, BP 156, 38042 Grenoble Cedex 9, France*

Received 4 May 2004; received in revised form 4 May 2004; accepted 5 June 2004

Available online 11 August 2004

Abstract

$(U_2O)(PO_4)_2$ is related to ultra-low expansion β-$(Zr_2O)(PO_4)_2$ ceramics, but shows a continuous thermal contraction. High-temperature neutron diffraction has allowed to follow accurately the thermal variations of its cell edges and to give a structural explanation to the phenomenon: like in β-$(Zr_2O)(PO_4)_2$, the dilatometric anomaly arises simultaneously from a contractive push–pull effect due to Coulombic repulsions and from a libration of the PO_4 and UO_7 polyhedra, but in the present case, the second mechanism predominates. The size of the tetravalent cation appears as a key parameter in monitoring the thermal expansion of ceramics of this family.

Keywords: Negative thermal expansion; Neutron diffraction; Crystalline oxides; Ceramics

1. Introduction

$(U_2O)(PO_4)_2$ belongs to a reduced family of isostructural tetravalent metal oxide phosphates of general formula $(M_2O)(PO_4)_2$. The archetype of the structure is the high-temperature orthorhombic variety of $(Zr_2O)(PO_4)_2$ (β-form) [1], also famous for its ultra-low thermal expansion ($\alpha_l = 1.5 \times 10^{-6}\,K^{-1}$) [2], and possible applications as thermal-shock resistant ceramics [3] and composites [4]. The numbering of the oxygen atoms in the following is same as for $(Zr_2O)(PO_4)_2$ in order to make comparisons easy. The structure (Fig. 1) is made up of distorted MO_7 pentagonal bipyramids tightly connected by pairs in the (100) plane by strong M–O(3)–M bridging, and forming infinite zigzag chains along [100] by sharing O(1)–O(1) edges. The UO_7 polyhedron shares oxygens O(2), O(4), and an O(1)–O(1) edge with three equivalent PO_4 tetrahedra.

$(U_2O)(PO_4)_2$ (space group *Cmca*, $a = 7.0878(5)$ Å, $b = 9.0362(8)$ Å, $c = 12.702(1)$ Å, $Z = 4$) is very similar to its Zr^{IV} counterpart [5,6], although the tetravalent cation is bigger ($r(Zr^{IV}) = 0.78$ Å, $r(U^{IV}) = 0.95$ Å in 7-fold coordination) [7].

This structure is likely to host other tetravalent actinide cations as Np^{IV} [8], or Th^{IV} (Fig. 2), but $(Th_2O)(PO_4)_2$ decomposes to $Th_4(PO_4)_4(P_2O_7)$ and ThO_2 above 1000°C. Pa^{IV} has the same ionic radius as U^{IV}, but tends to oxidize at high temperature, so the annealing of α-$Pa^{IV}P_2O_7$ at 900–1300°C yields $(Pa^{V}O)_4(P_2O_7)_3$ instead of the expected $(Pa_2O)(PO_4)_2$ [9]. On the contrary, Pu^{IV} reduces readily at high temperature and leads to monazite-like $Pu^{III}PO_4$.

Chernorukov et al. [10] report a very similar powder pattern for $(Hf_2O)(PO_4)_2$, but our attempts to reproduce their synthesis with a high-purity hafnium reagent only yielded the α-form, that is, an isotype of the low-temperature variety of $(Zr_2O)(PO_4)_2$. However, we observed a β-type solid solution between both compounds, extending up to high rates of hafnium. No such form is known for smaller tetravalent cations as tin or titanium.

In an early investigation of the thermal expansion of ceramics in the system UO_2–UP_2O_7, Kirchner et al.

*Corresponding author. Fax: +33-1-44-27-25-48.
E-mail address: gw@ccr.jussieu.fr (G. Wallez).

0022-4596/$ - see front matter © 2004 Elsevier Inc. All rights reserved.
doi:10.1016/j.jssc.2004.06.014

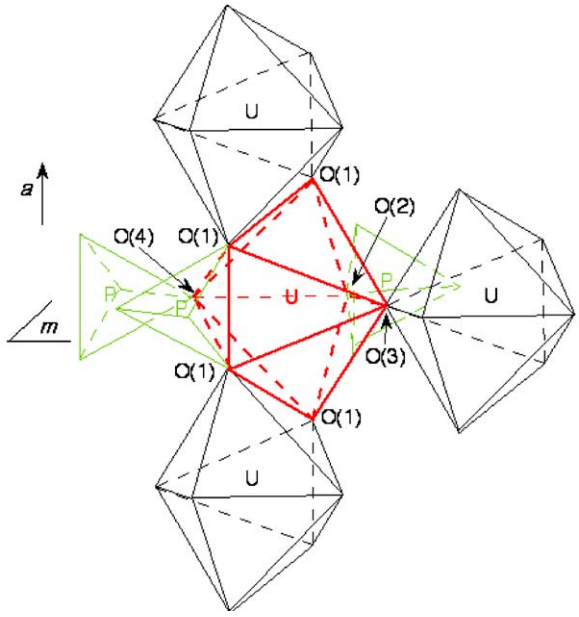

Fig. 1. Array of the UO_7 and PO_4 polyhedra in $(U_2O)(PO_4)_2$.

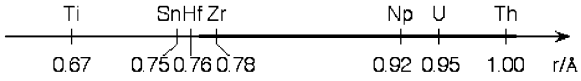

Fig. 2. Domain of existence of the β-$(Zr_2O)(PO_4)_2$ form for $(M_2^{IV}O)(PO_4)_2$ compounds (thick line) vs ionic radius of M^{IV} in seven-fold coordination [7].

report that sintered rods of "$(UO)_2P_2O_7$" (a misformulation for $(U_2O)(PO_4)_2$) show a continuous negative macroscopic expansion in the 20–1000°C range [11]. The aim of the present work is to give a structural explanation for this rare phenomenon by diffraction. Then, by drawing a parallel with the recently investigated ultra-low expansion material β-$(Zr_2O)(PO_4)_2$ [12], we will try to correlate the size of the tetravalent element with the expansion coefficient.

2. Experimental procedures and results

2.1. Synthesis

A concentrated solution of tetravalent uranium ($c_U \approx 1$ M) was first prepared by dissolution of uranium metal chips in 6 M HCl. A mixture containing tetravalent uranium and phosphate (added from 5 M H_3PO_4) in the mole ratio $U/PO_4 = 1$ was evaporated, then annealed under argon flow to prevent the oxidation of final $(U_2O)(PO_4)_2$ (from 300°C on) into triclinic $U^{IV}(U^{VI}O_2)(PO_4)_2$ [13]. The same kind of synthesis was performed in air at 1170°C to obtain a pure sample of the latter compound.

2.2. High-temperature diffraction

A $(U_2O)(PO_4)_2$ sample was put in a vanadium air-tight container and heated at 20°C, 120°C, 240°C, 360°C, 480°C and 600°C for powder neutron diffraction (HTND) on the D2B beamline of the Institut Laue-Langevin (Grenoble, France) with $\lambda = 1.5938$ Å (Ge monochromator). 445 independent reflections have been measured ($10° < 2\theta < 157°$). A subsidiary study on a $U(UO_2)(PO_4)_2$ sample was performed by high-temperature X-ray diffraction (HTXRD) at 20°C, 200°C, 400°C, and 800°C on a 17-cm vertical Philips PW1050/25 goniometer fitted with a heating platinum–rhodium 40% holder, using Ni-filtered Cu$K\alpha$ radiation. 468 independent reflections were measured ($30° < 2\theta < 80°$). This work was designed to follow the thermal expansion of the oxidized form of the title compound.

2.3. Rietveld refinements

The Fullprof.2k program [14] was run, using the crystal data of [5] as starting values for $(U_2O)(PO_4)_2$ (Fig. 3). The HTND background was interpolated from selected points. The refined data set included 3 cell parameters, the zero point, the Gaussian–Lorentzian shape factor, 3 coefficients of the *fwhm* Cagliotti's polynomial, 2 asymmetry parameters and the overall scale factor, 11 atomic coordinates and the 26 anisotropic displacement parameters. No distance or angle constraint was applied. The refinements led to the following reliability factors:

$$0.036 \leqslant R_P = \sum |y_o^i - y_c^i| / \sum y_o^i \leqslant 0.041$$

$$0.047 \leqslant R_{WP}(\text{id., weighted}) \leqslant 0.053$$

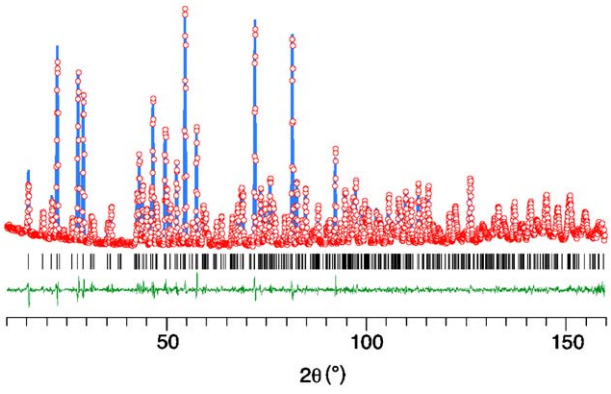

Fig. 3. Rietveld plot of neutron pattern for $(U_2O)(PO_4)_2$ at 20°C: observed (circles), calculated (solid, upper plot), difference (solid, lower plot) and angular positions of Bragg reflections (bars).

$$0.030 \leqslant R_{\mathrm{Bragg}} = \sum |I_o^i - I_c^i| / \sum I_o^i \leqslant 0.044$$

$$0.022 \leqslant R_F = \sum |(I_o^i)^{1/2} - (I_c^i)^{1/2}| / \sum (I_o^i)^{1/2} \leqslant 0.036.$$

The plots of the relative thermal variation of the cell edges (Fig. 4) show continuous evolutions. The linear expansion coefficients (Table 1) rank themselves as for β-$(Zr_2O)(PO_4)_2$ [12] and account for similar atomic displacements; however, they are systematically lesser and result in a negative definite overall expansion. The discrepancy between this last value and that given by Kirchner et al. [11], will be discussed thereafter. The HTXRD patterns of $U(UO_2)(PO_4)_2$ were treated in Le Bail's mode to refine the cell edges. The linear expansion coefficients of this compound are also reported in Table 1.

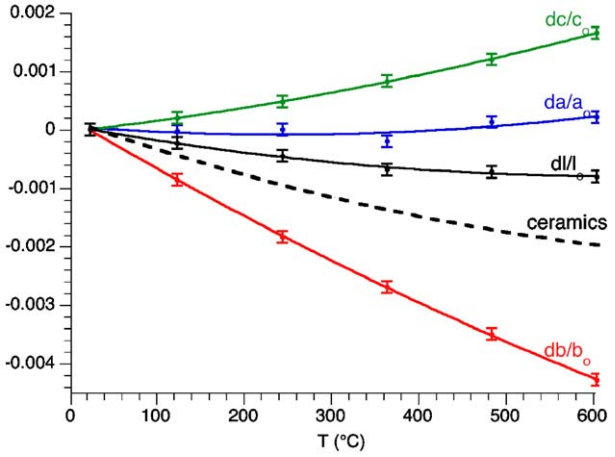

Fig. 4. Thermal linear relative expansion of $(U_2O)(PO_4)_2$ along the *a*, *b* and *c* axes; mean linear expansion of the cell (*l*). Dilatometric curve of the ceramics in dashed line [11].

From a structural point of view, the U–O and P–O distances obtained at 20°C (Table 2) are in good agreement with those previously published and show continuous evolutions on heating (Fig. 5). Their thermal expansion coefficients have been computed by linear fit (Table 2).

3. Discussion

The difference between the behaviors of $(U_2O)(PO_4)_2$ and β-$(Zr_2O)(PO_4)_2$ can be explained by comparing the magnitudes of the two simultaneous expansion-ruling

Table 1
Thermal linear expansion coefficients for $(U_2O)(PO_4)_2$ (HTND, this work, and dilatometry [11]), β-$(Zr_2O)(PO_4)_2$ (HTND [12]) and $U(UO_2)(PO_4)_2$ (HTXRD, this work) in the 20–600°C range

	$\alpha_a/10^{-6}\,K^{-1}$	$\alpha_b/10^{-6}\,K^{-1}$	$\alpha_c/10^{-6}\,K^{-1}$	$\alpha_l = (\alpha_a + \alpha_b + \alpha_c)/3/10^{-6}\,K^{-1}$
$(U_2O)(PO_4)_2$	+0.3	−7.4	+2.8	−1.4
$(U_2O)(PO_4)_2$, dilatometry				−3.3
β-$(Zr_2O)(PO_4)_2$	+3.9	−3.6	+4.3	+1.5
$U(UO_2)(PO_4)_2$	+1.5	+5.4	+1.0	+2.6

Table 2
U–O and P–O distances for the UO_7 and PO_4 polyhedra of $(U_2O)(PO_4)_2$ from powder neutron diffraction data at 20 and 600°C, thermal expansion coefficient of interatomic distances compared with the equivalent coefficient for $(Zr_2O)(PO_4)_2$

	$(U_2O)(PO_4)_2$ 20°C	$(U_2O)(PO_4)_2$, this work			$(Zr_2O)(PO_4)_2$
	Distances/Å in Bénard et al. [5]	Distances/Å		th. exp./$10^{-6}\,K^{-1}$	th. exp./$10^{-6}\,K^{-1}$
		20°C	600°C		
M–O(1) (2×)	2.371(2)	2.363(2)	2.361(2)	−2(1)	+6(1)
M–O(1) (2×)	2.514(3)	2.510(2)	2.534(2)	+17(1)	+20(2)
M–O(2)	2.235(4)	2.246(2)	2.232(3)	−10(1)	−6(2)
M–O(3)	2.078(2)	2.080(1)	2.071(1)	−8(1)	−3(1)
M–O(4)	2.248(4)	2.227(2)	2.231(3)	+4(1)	−5(2)
O(1)–O(1) edge of PO_4	3.933(3)	3.932(2)	3.926(2)	−3(1)	−2(1)
P–O(1) (2×)	1.543(3)	1.550(2)	1.552(2)	+2(2)	−5(2)
P–O(2)	1.515(5)	1.501(3)	1.495(4)	−6(2)	−7(3)
P–O(4)	1.515(5)	1.522(3)	1.507(4)	−17(2)	−3(3)
M–P sharing O(1)	3.768(2)	3.765(1)	3.763(1)	−1(1)	+1(1)
M–P sharing O(1)–O(1)	3.168(5)	3.170(3)	3.198(3)	+15(2)	+16(2)
M–*M* sharing O(1)–O(1)	4.040(2)	4.036(1)	4.053(1)	+7(1)	+12(2)
M–P sharing O(2)	3.761(4)	3.744(3)	3.725(3)	−9(1)	16(2)
M–*M* sharing O(3)	4.156(3)	4.159(2)	4.141(2)	−8(1)	−3(1)
M–P sharing O(4)	3.736(5)	3.736(3)	3.725(3)	−5(2)	−4(3)

M stands for U or Zr.

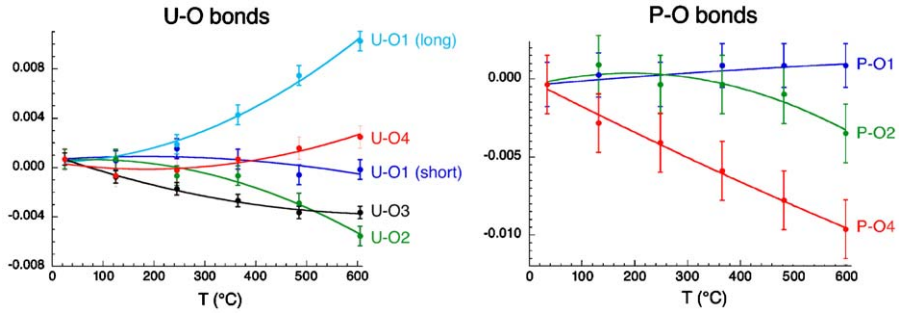

Fig. 5. Relative thermal expansion of U–O (left) and P–O (right) bond lengths ($(l–l_o)/l_o = f(T)$).

mechanisms we reported previously for the zirconium compound [12].

3.1. Cation repulsions

The short distance between neighbor M^{IV} cations of consecutive (001) layers sharing an O(1)–O(1) edge (Table 2) induces Coulombic repulsions that relax by a rotation movement of the *M*–O–*M* linear bridgings in the (100) planes, taking the central oxygen anion (O(3) on inversion center) as a pivot (Fig. 6). Similarly, repulsions arise between M^{IV} and P^{V} cations of the same layer sharing another O(1)–O(1) edge, that tend to expand the *M*–P distance also at a high rate and to contract the O(1)–O(1) edge (*M*–P distance and O(1)–O(1) edge of PO_4 in Table 2). The resulting push–pull mechanism along the *M*–O(2) and *M*–O(4) bonds shifts the neighbor PO_4 tetrahedra towards empty spaces of the structure, leading to a more compact array of atoms. This phenomenon plays a major role in inhibiting the thermal expansion of β-$(Zr_2O)(PO_4)_2$ along the *b*-axis, but appears negligible in the uranium compound, insofar as the expansion rate of the U–U distance is much lower than the Zr–Zr one ($7 \times 10^{-6}\,K^{-1}$ instead of $12 \times 10^{-6}\,K^{-1}$), thus reducing the driving force of the push–pull mechanism. This fact is in agreement with the expected attenuation of the Coulombic repulsions while distance increases ($d_{U-U} = 4.040(2)$ Å instead of $d_{Zr-Zr} = 3.717(1)$ Å at 20°C) and the lesser stiffness of the oxygen framework in the uranium compound due to weaker *M*–O bonds.

3.2. Oxygen liberation

Simultaneously, the 2-fold coordinated oxygens involved in nearly linear bridgings (U–O(3)–U; U–O(2)–P; U–O(4)–P) in the (*b*,*c*) plane oscillate perpendicular to their bonds as shown by the transverse elongation of the thermal ellipsoids at 600°C (Fig. 7), thus reducing the distances between cations (Table 2, 3 last lines). The phenomenon affects the three bridgings nearly alike, but the contraction of the U–O–P ones is asymmetric: the

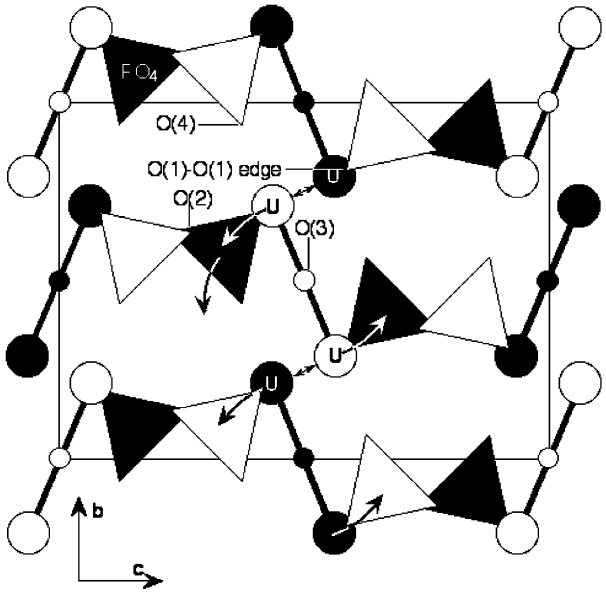

Fig. 6. (100) projection of the structure showing the push–pull mechanism generated by the U^{IV}–U^{IV} repulsions. Atoms/tetrahedra at/near $z = 1/2$ are in white; those at/near $z = 0$ are in black.

strength of the P–O(4) bond increases while the U–O(4) one decreases whereas the P–O(2) bond shows a stronger shrinkage than the U–O(2) one. This contractive mechanism appears somewhat related to the classical rocking effect observed for compounds with monodentate frameworks as α-ZrP_2O_7 [16], ZrW_2O_8 [17], or $NbZr(PO_4)_3$ [18], and considered today as the most successful way to achieve ultra-low or negative thermal expansion [19]. However, the case of the $(M_2O)(PO_4)_2$ structure is somewhat different insofar as the 3-fold (1P + 2 M) coordination of oxygen O(1) is unfavorable for polyhedra librations. Because O(1) is only free to move perpendicular to the plane of its neighbors, its thermal ellipsoid is stretched, unlike those of the other oxygens, that flatten perpendicular to the cations axis (Fig. 7). The polyhedra cannot behave as rigid units (at variance with some monodentate structures) insofar as the oxygen atoms have different degrees

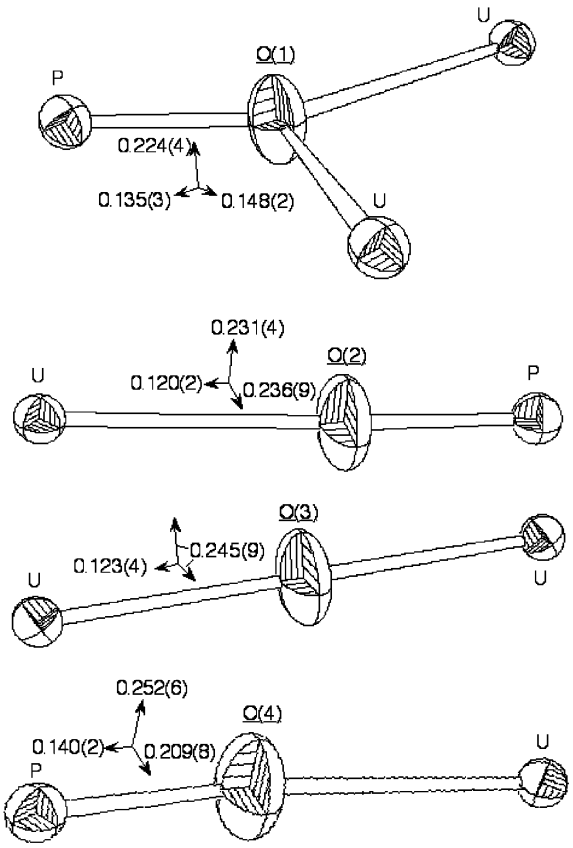

Fig. 7. U–O–U and U–O–P bridging at 600°C (50% probability thermal ellipsoids by Ortep [15]) with mean atomic displacements of oxygen atoms/Å. Note the elongation of the O(1) ellipsoid perpendicular to the (U,U,P) plane and the flattening of the other ones following the cations axis.

of freedom, so the movements of the latter should rather be thought of as individual and loosely correlated phenomena. Nevertheless, the unidirectional transverse movement of O(1) allows to nearly nullify the expansion of both the P–O(1) and the short U–O(1) bonds, while the long U–O(1) one expands strongly as a result of the Coulombic repulsion with the edge-sharing cation P^V.

As shown on Fig. 1, the *a*-parameter depends roughly on the sum of the lengths of the O(1)–O(1) edge of the PO_4 tetrahedron and the short U–O(1) bond. Their near-zero expansion is in good agreement with that of the *a*-edge, the slight difference resulting probably from the positive contribution of the long U–O(1) bonds. Similarly, the negative expansion of the nearly *b*-directed U–O(3)–U and U–O(4)–P bridgings (Fig. 6) generates a strongly negative-definite α_b coefficient; while along the *c*-axis, the positive expansion of the long U–O(1)–P bridgings is partly offset by the shrinkage of the U–O(2)–P one. In terms of mean atomic displacement, it appears that the transverse librations of the oxygen atoms are stronger in $(U_2O)(PO_4)_2$ than in its zirconium counterpart (+20% for O(1), +16% for O(2), +17% for O(3), +10% for O(4)), in agreement with the larger size of the U^{IV} cation that gives to the U–O bonds a higher ionicity and a lesser strength. This is the reason why the contraction of the strongest bonds is more efficient in the present compound.

The mean linear expansion coefficient of $(Zr_2O)(PO_4)_2$ obtained by powder diffraction was in good agreement with that of a ceramics ($\alpha_l = 1.5 \times 10^{-6}\,K^{-1}$ for both) [12]. On the contrary, there is a notable discrepancy between our HTND measurements and the dilatometric behavior [11] of $(U_2O)(PO_4)_2$ obtained by Kirchner et al. (Fig. 4, Table 1). In order to try to explain it, we first considered the possibility that all or part of the $(U_2O)(PO_4)_2$ sample of these authors had been oxidized into $U^{IV}(U^{VI}O_2)(PO_4)_2$ when heating, as occurs even under low oxygen pressure. Actually, this reaction would result in a +0.8% linear expansion of the material according to the volumes of the formula units [5,20], not in a contraction. Neither does the subsidiary HTXRD study of the oxidized form give a satisfactory answer, insofar as its overall expansion coefficient appears low, but positive definite. So, a part of the negative expansion of the ceramics results probably from extrinsic microstructural features as cracks, which commonly affect the overall expansion of materials made up of anisotropically expanding crystallites. A "late" sintering effect is unprobable insofar as even at moderate temperatures, the contraction is stronger than expected.

Beside its theoretical aspect, this study aims a practical outcome: the improvement of the thermal properties of $(Zr_2O)(PO_4)_2$ ceramics. Actually, we now know that partial substitutions of bigger cations to Zr^{IV} should result in reducing the dilatometric behavior to the ideal zero-expansion. However, the lack of non-toxic tetravalent cations larger than Zr^{IV} inclines us to replace it with cations of lower oxidation state and to balance the charge deficit by substituting hexavalent cations to P^V. Investigations are now underways in this direction. More generally, it appears reasonable to consider cations substitutions in already known monodentate or quasi-monodentate oxide frameworks in order to modulate their thermal expansion in a similar way.

4. Conclusion

$(U_2O)(PO_4)_2$ undergoes a continuous negative thermal expansion resulting mainly from a pseudo polyhedra-rocking mechanism. A bond-by-bond comparison with the isotypic ultra-low expansion material *β*-$(Zr_2O)(PO_4)_2$ proves that the higher ionicity and lower stiffness of the U–O bonds compared to the Zr–O ones is responsible for the magnification of the contracting effect.

Acknowledgments

The authors are grateful to Peter Cross (Institut Laue-Langevin) for the HTND measurements.

References

[1] W. Gebert, E. Tillmanns, Acta Crystallogr. B 31 (1975) 1768.
[2] I. Yamai, T.J. Oota, Am. Ceram. Soc. 68 (1985) 273.
[3] W. Schreyer, J.F. Schairer, J. Petrology 2 (1961) 324.
[4] B.A. Bender, T.L. Jessen, S. Browning, Ceram. Eng. Sci. Prod. 16 (1995) 613.
[5] P. Bénard, D. Louër, N. Dacheux, V. Brandel, M. Genet, Anal. Quim. 92 (1996) 79.
[6] J.H. Albering, W. Jeitschko, Z. Kristallogr. 210 (1995) 878.
[7] R.D. Shannon, Acta Crystallogr. A 32 (1976) 751.
[8] N. Dacheux, A.C. Thomas, V. Brandel, M. Genet. J. Nucl. Mater. 257 (1998) 108.
[9] C.E. Bamberger, in: A.J. Freeman, C. Keller (Eds.), Handbook on the Physics and Chemistry of the Actinides, Vol. 3, Elsevier, Amsterdam, 1985, p. 289.
[10] N.G. Chernorukov, I.A. Korshunov, M.I. Zhuk, Russ. J. Inorg. Chem. 28 (1983) 934.
[11] H.P. Kirchner, K.M. Merz, W.R. Brown, J. Am. Ceram. Soc. 46 (1963) 137.
[12] G. Wallez, S. Launay, J.P. Souron, M. Quarton, E. Suard, Chem. Mater. 15 (2003) 3793.
[13] V. Brandel, N. Dacheux, M. Genet, R. Podor, J. Solid State Chem. 159 (2001) 139.
[14] J. Rodriguez-Carvajal, Fullprof.2k: Rietveld, profile matching and integrated intensity refinement of X-ray and neutron data, V 1.9, Laboratoire Léon Brillouin, CEA, Saclay, France, 2001.
[15] M.N. Burnett, C.K. Johnson, ORTEP-III: Oak Ridge Thermal Ellipsoid Plot Program for Crystal Structure Illustration, Oak Ridge National Laboratory Report ORNL-6895, 1996.
[16] N. Khosrovani, V. Korthuis, A.W. Sleight, Inorg. Chem. 35 (1996) 485.
[17] T.A. Mary, J.S.O. Evans, A.W. Sleight, T. Vogt, Science 272 (1996) 90.
[18] K.V.G. Kutty, R. Asuvathraman, C.K. Mathews, V.V. Varadaraju, Mater. Res. Bull. 29 (1994) 1009.
[19] A.W. Sleight, Inorg. Chem. 37 (1998) 2854.
[20] P. Bénard, D. Louër, N. Dacheux, V. Brandel, M. Genet, Chem. Mater. 6 (1994) 1049.